Earthquake Geotechnical Engineering for Protection and Development of Environment and Constructions – Silvestri & Moraci (Eds)
© 2019 Associazione Geotecnica Italiana, Rome, Italy, ISBN 978-0-367-14328-2

Centrifuge tests to evaluate dynamic impedance functions of square surface foundation

A. Borghei & M. Ghayoomi
The University of New Hampshire, Durham, NH, USA

ABSTRACT: The lateral and rocking impedance functions of a structure with a mat foundation of 3.5-m width under earthquake motions were determined by conducting dynamic centrifuge experiments. A physical model, representing the structure at 50-g centripetal acceleration, was placed on a layer of dry soil, and was excited with four different intensity of a historical earthquake. Compared to the lateral and rocking theoretical impedance functions for circular massless foundation on surface of an elastic half-space soil layer, the experimental foundation stiffness values are lower, while the experimental foundation dashpot coefficients are larger. Results from different seismic events reveal that as the maximum soil shear strain increases, the lateral and rocking foundation stiffness decrease, while the lateral dashpot coefficient increases. Furthermore, no general trend of increase or decrease was observed for the rocking dashpot coefficient. More experiments are planned to further investigate the subject.

1 INTRODUCTION

Soil properties underneath shallow foundations would significantly affect buildings' seismic response during earthquake events (Luco & Wong 1986, Veletsos et al. 1997, Stewart et al. 1999, Borghei & Ghayoomi 2018b). Terms such as Soil-Structure Interaction (SSI) and Soil-Foundation-Structure Interaction (SFSI) are commonly used in the literature to describe the interaction between the structure, foundation, and surrounding soils. This interaction is mainly caused by two mechanisms; i.e. inertial and kinematic interaction (Wolf 1985, Stewart et al. 1999). The focus of this paper is on inertial interaction.

Inertial and kinematic interactions occur concurrently. As a result, a motion measured at the foundation level, commonly called Foundation Motion (FM), diverges from a motion measured at the ground surface and far from the structure, named Free-Field or Far-Field Motion (FFM). Due to kinematic interaction, the amplitude of the lateral component of FM decreases compared to FFM and the rocking and torsional components of FM are introduced (Veletsos & Prasad 1989, Veletsos et al. 1997, Kim & Stewart 2003, Borghei & Ghayoomi 2018a). Inertial forces caused by movements in components of the structure, lead to relative displacement and rotation between FM and FFM (NEHRP CJV 2012).

In substructure approaches, performed to evaluate SSI effects, inertial interaction is impacted by foundation impedance functions. Impedance functions describe the stiffness and damping of the soil beneath a foundation. The majority of the previous researches on foundation impedance functions are based on analytical and numerical analyses (Veletsos & Wei 1971, Apsel & Luco 1987), and experimental studies on this subject are limited. Furthermore, most of these experimental studies were performed by conducting forced foundation vibration tests (Lin & Jennings 1984, Crouse et al. 1985, Wong et al. 1988, Crouse et al. 1990). Although these experiments provided valuable information about the impedance functions, forced vibration may not adequately represent the response to earthquake excitations (Lin & Jennings 1984). Very limited number of experimental research assessed impedance functions for foundations under seismic motions (Moslem & Trifunac 1986, Kim 2001). There are two main challenges that should be addressed for estimating the foundation impedance functions during an earthquake event. First,

response time histories of the structure and FFM should be recorded, and the motions should be synchronized to decrease undesirable time lags between motions. Second, the difference between FFM and FM should be evaluated. Commonly, amplitudes of these motions are relatively low; as a result, the motion may have low signal-to-noise ratio (Kim 2001). In this research, these challenges are met by conducting centrifuge modeling. Structural motions and FFM were measured by an array of accelerometers. To remove the undesirable lag between the measured motions, the accelerometers were connected to a single data acquisition system. Moreover, the difference between FFMs and FMs, measured during the dynamic experiment, have sufficient signal-to-noise ratio to evaluate the impedance functions.

This paper focuses on preliminary results of a set of centrifuge tests to experimentally estimate lateral and rocking impedance functions of a target structure with a mat foundation placed on surface of a sandy soil during a suite of earthquake motions. A Single-Degree of Freedom (SDOF) physical model, representing the target structure, was placed on a layer of dry sand within a laminar container. The response of the system under a suite of ground motions was analyzed to estimate the foundation impedance functions. The experimental functions were also compared with a theoretical impedance functions available in the literature.

2 BACKGROUND

The relationships between inertial forces such as base shear and moment at the foundation level and the relative foundation displacement and rotation with respect to FFM are driven by foundation impedance functions. Equation (1) describes the lateral, rocking, and coupling lateral-rocking foundation impedance functions. These functions are frequency-dependent and complex-valued. The real and imaginary parts of the functions represent the stiffness and damping of the foundation support medium, respectively (Veletsos & Wei 1971, Apsel & Luco 1987, NEHRP CJV 2012).

$$\hat{k}_j = k_j + i\omega c_j \qquad j = u,\ \theta,\ u\theta,\ \theta u \tag{1}$$

$$k_j = \alpha_j K_j;\ c_j = \beta_j \frac{K_j r_j}{V_s}\ j = u,\ \theta,\ u\theta,\ \theta u \tag{2}$$

$$r_u = \sqrt{\frac{A_f}{\pi}};\ r_\theta = \sqrt[4]{\frac{4I_f}{4}};\ r_{u\theta} = r_{\theta u} \cong r_u \tag{3}$$

where subscript j denotes either lateral deformation mode (u), rocking deformation mode (θ), or coupling lateral-rocking deformation modes ($u\theta$ and θu); k_j and c_j are frequency-dependent foundation stiffness and dashpot coefficients, for mode j; i is the square root of -1; ω is the circular frequency (rad/s). The frequency dependent stiffness and dashpot coefficients (i.e. k_j and c_j, respectively) for a foundation can be estimated using Equation (2); where K_j is the static stiffness of a foundation, for mode j; α_j and β_j control the frequency dependency of stiffness and damping terms; V_s is an average reduced shear wave velocity of the soil beneath the foundation; r_j is an equivalent foundation radius, for mode j. The static stiffness of foundations with different geometries are readily available in the literature (NEHRP CJV 2012); moreover, the α_j and β_j terms are conventionally determined by performing numerical calculations or estimated based on available numerical studies on the literature (Veletsos & Wei 1971, Wong & Luco 1985, Apsel & Luco 1987, NEHRP CJV 2012). r_u, r_θ, and $r_{u\theta}$ ($r_{\theta u}$) are equivalent foundation radius for lateral deformation, rocking deformation, and coupling deformation modes, respectively, expressed in Equation (3).

Crouse & McGuire (2001) developed a generic SFSI model that includes a multi-degree of freedom structure with translational and rocking impedance functions. This model was used in this paper to estimate the impedance functions for a SDOF system. Moslem & Trifunac (1986) described a procedure, used in this paper, to estimate impedance functions based on measured

acceleration time histories and properties of the structure, and by equating the base shear and moment generated at the foundation due to the inertial interaction with lateral force and rocking moment in the impedance functions. To estimate the impedance functions, two equations for lateral and rocking motions should be solved for three unknowns; i.e. $\hat{k}_u$, $\hat{k}_\theta$, and $\hat{k}_{u\theta} = \hat{k}_{\theta u}$. Therefore, the system of equations does not have a unique solution, so the ratios of $\hat{k}_{u\theta}/\hat{k}_u$ and $\hat{k}_{\theta u}/\hat{k}_\theta$ should be either estimated (Veletsos & Wei 1971, Wong & Luco 1985, Apsel & Luco 1987) or assumed negligible. The analytical evaluations of impedance functions have shown that for rigid surface foundations on half-space, these impedance function ratios are negligible (Moslem & Trifunac 1986), which was also applied in this investigation.

3 EXPERIMENTAL PROGRAM

3.1 *Geotechnical centrifuge and soil material*

A set of dynamic centrifuge tests was performed using the 5 g-ton (1-m radius) geotechnical centrifuge facility at the University of New Hampshire (Ghayoomi & Wadsworth 2014). F-75 silica sand, a poorly graded Sand (SP based on USCS classification), was used as the soil material with D_{50} of 0.19 mm, the coefficient of uniformity, C_u, of 1.74, and the coefficient of curvature, C_c, of 1.07 (ASTM D2487-11 2011), and maximum and minimum void ratios of 0.8 and 0.49, respectively (Mirshekari et al. 2018). The dry pluviation technique was used to prepare the soil in a laminar container with a relative density of about 60%. The achieved relative density and soil dry density were measured as 62.6%, and 1650.2 kg/m^3, respectively. The laminar container was used to allow the soil to deform in the shear-beam mode with minimal undesirable boundary effects (Hushmand et al. 1988). The width, length, and depth of the laminar container are 17.7 cm, 35.6 cm, and 24.1 cm, respectively.

Small-strain shear modulus, G_{max}, of sandy soils is approximately proportional to the square root of the effective stress. Therefore, the small-strain shear wave velocity of sandy soils increases with depth; moreover, the weight of a structure increases the effective stress beneath the foundation. Stewart et al. (2003) recommend using a harmonic mean to calculate an average small-strain shear wave velocity from the bottom of the foundation to an effective depth, which is about half the foundation width for a square foundation. In this study, the relation between the effective stress and the small-strain shear modulus of the soil was estimated by using an equation suggested by Seed & Idriss (1970) for clean sands. Moreover, an equation developed by Poulos & Davis (1974) for induced vertical stress beneath the center of square loaded area was used to consider the increase of effective stress due to the weight of the structure. The average small-strain shear wave velocity of the soil in the free field and beneath the structure, from the soil surface to the depth equal to the foundation half width, were estimated as 127 and 254 m/s, respectively. Further, the shear modulus reduction function by Menq (2003), shown in Equation (4), was used calculate strain-dependent modulus. In Equation (4), the reference strain, γ_r, and the curvature coefficient, a, were estimated as 0.037%, and 0.78, respectively, for the soil used in the research at the depth about half of the foundation width.

$$\frac{\mathrm{G}}{\mathrm{G_{max}}} = \frac{1}{1 + \left(\frac{\gamma}{\gamma_r}\right)^{\mathrm{a}}} \tag{4}$$

3.2 *Design of physical models*

A SDOF mass-foundation physical model system, representing a simplified 4-story concrete structure with a 1-m thick surface mat foundation in the 50-g centripetal acceleration, was designed and built. The dimensions of the laminar container limits the width of the mat foundation to 3.5 m. The foundation width, bearing pressure, fundamental natural frequency, and structural-to-foundation mass ratio were considered in the design of physical models. The bearing pressure of the prototype structure was determined as 145 kPa, considering typical dead and live loads. The first fixed-base natural frequency of the prototype structure was picked as 3.36 Hz. The scaling factors of centrifuge experiments (Wood 2004) were used for

designing the physical model. Figure 1a shows the schematic layout and instrumentations used in the centrifuge experiment; moreover, Figure 1b demonstrates a photograph of the structural model.

Frequency response analyses were performed using Abaqus program (Simulia 2012) to estimate the natural frequencies of the structural model for design. Modal hammer test was done to measure the fixed-base natural frequency, f_{fix} of the model after construction as 168.3 Hz in the prototype scale (3.36 Hz in the model scale). The logarithmic decremented method (Chopra 1995) was used to estimate the structural system damping ratio of 0.32%.

Columns of the physical model were designed such that they remain elastic, while the physical model is excited by target seismic motions. Bearing capacity and settlement were estimated to ensure stability of the structural model during the centrifugation. Furthermore, the factor of safety against overturning was controlled, while the model is shaken by target seismic motions.

3.3 *Seismic motions*

Scaled versions of 1989 Loma Prieta earthquake motion recorded at the Santa Cruz station were selected as the desired motion. The in-flight shake table of the centrifuge was calibrated for four different intensities of the desired motion, based on the procedure developed by Mason et al. (2010). The Base motions (BMs), which are motions measured at the bottom of the soil layer, during the four seismic events with increasing intensities are called SCZ_1, SCZ_2, SCZ_3, and SCZ_4. The ground motion characteristics of BMs are tabulated in the prototype scale in Table 1. According to the table, while Peak Ground Acceleration (PGA) and Arias intensity of the motions were significantly increased, the mean period of the motions were approximately constant between the events. Therefore, the frequency content of the motions were approximately similar to each other, although the intensities were significantly different.

4 RESULT AND DISCUSSION

The lateral flexible-base natural frequency, $\widetilde{f_L}$, of the physical model under SCZ_1 was determined by calculating a transfer function between the lateral motion measured at the oscillator mass, called Structure Horizontal motion (SHM) and the lateral component of FM, as shown in Figure 2a. Furthermore, the rocking flexible-base natural frequency, $\widetilde{f_R}$, was also estimated

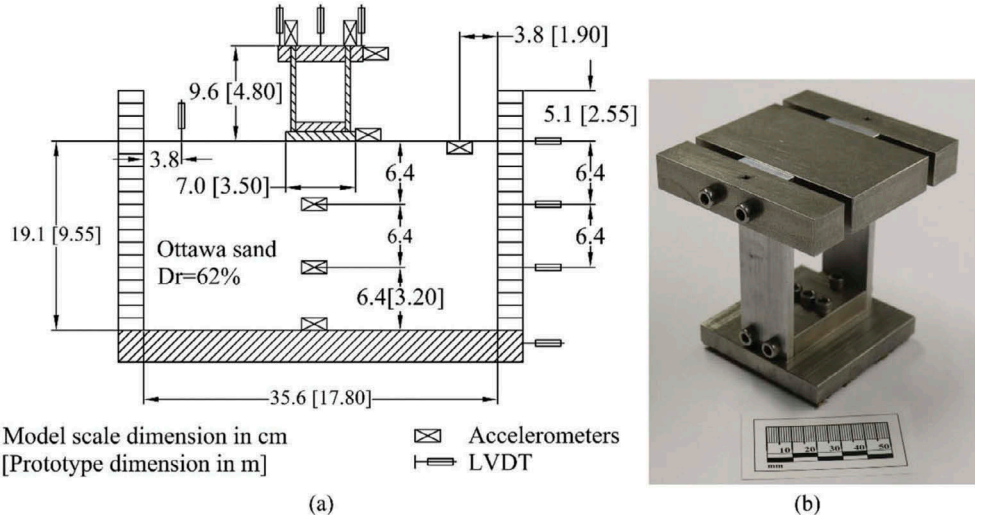

Figure 1. (a) Schematic and instrumentation layout of the centrifuge experiment; (b) photograph of the structure physical model.

Table 1. Ground motion characteristics of BMs and flexible-base natural frequencies of the system, during the seismic events. Results are presented in the prototype scale.

Event ID	Order	Ground motion Characteristics of BM			Flexible-base natural frequency and period lengthening		
		PGA (g)	I_a (m/s)	T_m (s)	$\tilde{f}_L(Hz)$	$\tilde{f}_R(Hz)$	$\tilde{T}/T$
SCZ_1	1	0.09	0.10	0.23	2.44	2.44	1.38
SCZ_2	2	0.23	1.01	0.24	2.25	2.22	1.50
SCZ_3	3	0.30	1.53	0.26	2.30	2.30	1.46
SCZ_4	4	0.40	3.70	0.26	2.00	2.00	1.68

PGA (Peak Ground Acceleration) is the maximum absolute value of acceleration time history.
I_a, Arias intensity, is calculated based on a method proposed by Arias (1970).
T_m, the mean period, is calculated based on a method suggested by Rathje et al. (1998).

using a transfer function between Foundation Rocking motion (FRM) and FM, as demonstrated in Figure 2b. FRM is the product of the foundation half-width and a rocking acceleration time history, estimated as the difference between the two vertical acceleration recordings on the opposite sides of the model divided by the distance between the accelerometers. Flexible-base natural frequencies of the model during the four seismic events are tabulated in Table 1. According to the table, as the intensity of the motion increases, the flexible-base natural frequencies of the structure decreases, as expected. The period lengthening, $\tilde{T}/T$,which is the ratio of the lateral flexible base period of the structure, $\tilde{T}$ to the fixed base period of the structure, T, was also calculated and shown in Table 1.

The theoretical impedance functions were calculated based on the model by Veletsos & Wei (1971) for the lateral and rocking impedance functions of a rigid massless circular foundation supported at the surface of an elastic half-space. The reduction of the shear modulus of the soil with the shear strain was considered when computing the theoretical impedance functions. To calculate a representative shear strain time history, the difference between displacement time histories measured at the soil surface and 6.4 m below the soil surface, see Figure 1, was divided by the distance between the two LVDTs. The maximum shear strain, γ_{max}, was defined as the maximum absolute value of the shear strain time history. Menq (2003) model, Equation (4), was used to reduce the average small-strain shear wave velocity of the soil under the structure, 254 m/s, according to the γ_{max} value. The average strain-reduced shear wave velocity of the soil below the foundation, V_s, was computed as 101 m/s, when the system was excited by SCZ_1 motion.

Figure 3 compares the theoretical and experimental impedance functions, when the structure was excited with SCZ_1 motion. The physical model mainly vibrates around its flexible-base natural frequencies; therefore, amplitudes of the structural motions for frequencies far from the flexible-base natural frequencies are relatively small, compared to amplitudes of the structural motions around the flexible-base natural frequency. Consequently, coherence of the experimental impedance functions are relatively low for frequencies far from the flexible-base natural frequency, as shown in Figure 3c and 3f. Hence, the estimated impedance functions are not reliable for these frequencies. In this study, the experimental impedance function values around the flexible-base natural frequencies with a frequency range of 0.5 Hz and coherence more than 0.8 are considered as reliable values, where these points are shown with

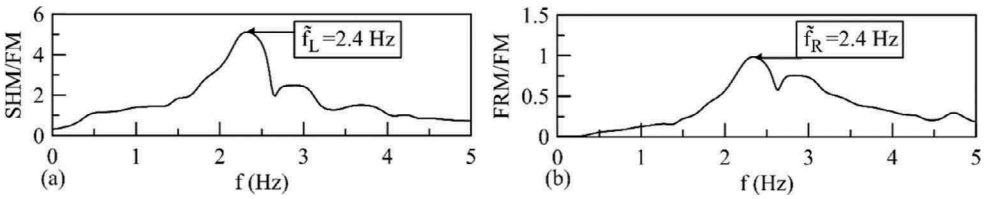

Figure 2. The transfer function of the physical model, when excited by the SCZ_1: (a) structure transfer function; (b) foundation rocking transfer function.

markers in the figure. Figure 3a and 3d demonstrate that the experimental lateral and rocking stiffness are smaller than the theoretical ones. However, Figure 3b and 3e illustrate that the experimental lateral and rocking dashpot coefficients are larger than the theoretical ones. The observed differences between the theoretical and experimental impedance functions could be due to: 1) the kinematic interaction is neglected in the theoretical impedance function; however, the kinematic and inertial interaction occur simultaneously in the experiment; 2) Veletsos & Wei assumed linear elastic behavior for the soil. As the lateral and rocking static stiffness, Equation (2), were calculated by considering reduction of shear modulus with shear strain, non-linearity of the soil may affect the lateral and rocking stiffness coefficients (α_u, and α_θ, respectively, see Equation (2)); 3) although the radiation damping is considered in the theoretical impedance function, soil damping is neglected. By considering the soil damping the lateral and rocking damping coefficients (β_u, and β_θ, respectively, see Equation (2)) may increase. For frequencies from zero to 4 Hz, the β_θ changes from zero to about 0.047 with an average of 0.022; as a result, the theoretical dashpot coefficient is significantly smaller than the experimental one, as shown in Figure 3e. It is worth mentioning that the static dashpot coefficient, $k_\theta\, r_\theta/V_s$, (see Equation (2)) is about 10.6 MN.m.r/rad, which is still smaller than the experimental dashpot coefficient; and 4) the theoretical impedance function was developed for semi-infinite soil layer; however the experimental soil layer is relatively thin. Kausel (1974) showed that the static stiffness values and stiffness and damping coefficients of a finite soil layer are different from those for a half-space soil layer. Hence, it is planned to compare the experimental impedance functions with more advanced theoretical impedance functions.

To evaluate the effect of intensity of the seismic motion on the experimental impedance functions, an average of the reliable impedance functions, shown with markers in Figure 3, was calculated. Figure 4 illustrates the effect of the maximum soil shear strain on the average experimental impedance functions, also compares them with the average of the theoretical impedance functions with frequencies from 1.5 Hz to 3 Hz. Figure 4a and 4c demonstrate that as the maximum shear strain in the soil increases, the experimental lateral and rocking stiffness generally decrease, with the same trend as the theoretical lateral and rocking stiffness. This behavior was expected, since as the shear strain increases the shear modulus of the soil decreases. Although it was predicted that the average lateral stiffness, $\bar{k}_u$, for the SCZ_4 motion would be smaller than that of the SCZ_3 motion, the experimental results showed that the $\bar{k}_u$ value for the SCZ_4 motion was slightly (13%) larger than the value for the SCZ_3 motion. The main reason for the observed discrepancy is that the relative density of the soil increased due to seismic induced settlement of the soil. As a result, the small-strain shear modulus of the soil increases, after each motion was applied to the system. More dynamic centrifuge experiments

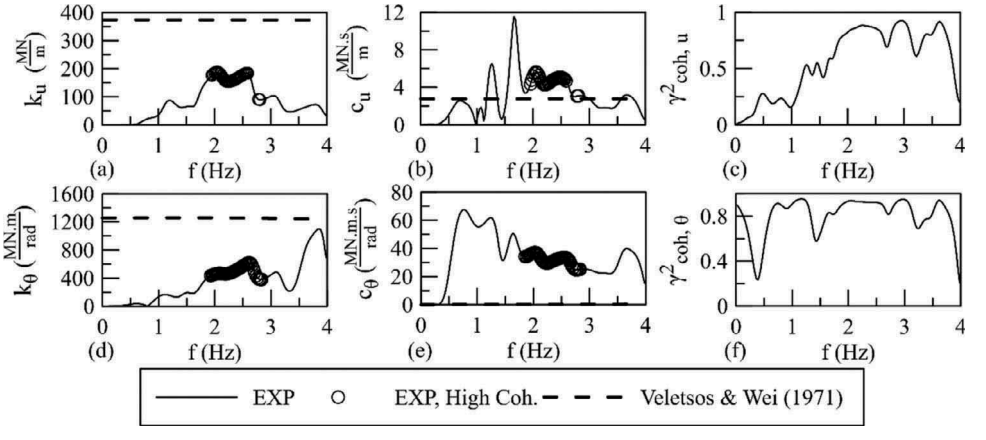

Figure 3. Comparison of the experimental impedance function of the physical model with the theoretical impedance function developed by Veletsos & Wei (1971), when it was excited with SCZ_1 motion: (a) lateral stiffness; (b) lateral dashpot coefficient; (c) coherence of lateral impedance function; (d) rocking stiffness; (e) rocking dashpot coefficient; (f) coherence of rocking impedance function.

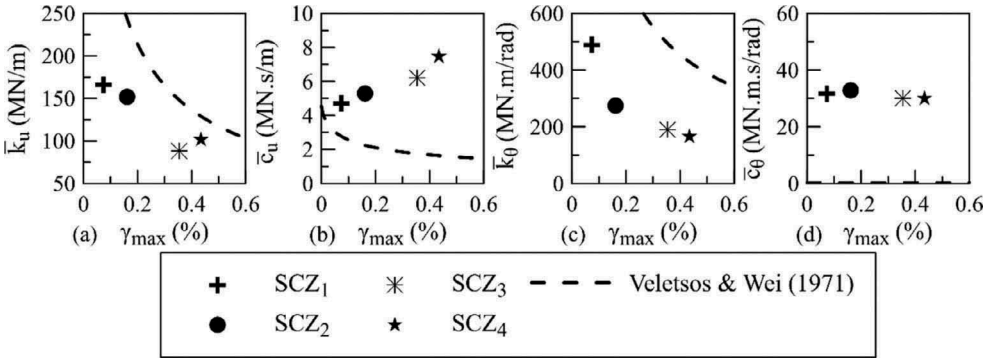

Figure 4. Effect of maximum shear strain of the soil during different seismic events on the average impedance functions and the theoretical impedance functions, developed by Veletsos & Wei (1971): (a) lateral stiffness; (b) lateral dashpot coefficient; (c) rocking stiffness; (d) rocking dashpot coefficient.

are planned to further investigate the observed trend. Figure 4b demonstrates that as the maximum shear strain increases, the experimental lateral dashpot coefficient increases. This behavior is also expected since the damping of the soil tends to increase by increasing the shear strain. The figure also illustrates that the trend for the lateral theoretical dashpot coefficient is different from the trend for the experimental values. The main reason is that the soil material damping is neglected in the theoretical impedance functions, and only the foundation radiation damping is considered in the theoretical impedance function, as previously mentioned. It was expected that the experimental rocking dashpot coefficient also increases by increasing the maximum shear strain, however it does not follow the expected behavior, as shown in Figure 4d. The change of the relative density of the soil could be one of the reasons for the discrepancy. Furthermore, the figure demonstrates that the experimental rocking dashpot coefficient values are significantly larger than the theoretical values, for the aforementioned reason. More experiments is planned to elaborate this behavior.

5 CONCLUSION

The lateral and rocking impedance functions of a model structure with a surface mat foundation with width of 3.5 m during earthquake events were experimentally evaluated by conducting a set of dynamic centrifuge experiments. The experimental impedance functions of a square mat foundation were compared with the theoretical impedance functions for a circular massless foundation on surface of a half space elastic soil layer. While the experiment lateral and rocking stiffness were smaller than the theoretical ones, the experimental lateral and rocking dashpot coefficient were larger. Results of the four seismic events demonstrate that as the maximum shear strain in soil increases, the lateral and rocking foundation stiffness decreases. However, the lateral dashpot coefficient increases and the rocking dashpot coefficient does not show any meaningful trend. More experiments is planned to further investigate these patterns.

REFERENCES

Apsel, R.J. & Luco, J.E. 1987. Impedance functions for foundations embedded in a layered medium: an integral equation approach. *Earthquake Engineering & Structural Dynamics* 15(2): 213–231.

Arias, A. 1970. A measure of earthquake intensity. *Seismic design for nuclear power plants* : 438–483.

ASTM D2487-11 2011. Standard practice for classification of soils for engineering purposes (Unified Soil Classification System) *ASTM International*: 1–12.

Borghei, A. & Ghayoomi, M. 2018a. Centrifuge modeling to evaluate kinematic soil-foundation-structure interaction. *5th Geotechnical Earthquake Engineering and Soil Dynamics (GEESDV)*, June 10–13, 2018. Austin, Texas, USA: ASCE.

Borghei, A. & Ghayoomi, M. 2018b. Experimental evaluation of two-stage scaling in physical modeling of soil-foundation-structure systems. *9th International Conference on Physical Modelling in Geotechnics (ICPMG)*, 17th - 20th July 2018. Leiden, the Netherlands: CRC Press Taylor & Francis Group.
Chopra, A.K. 1995. *Dynamics of structures: theory and applications to earthquake engineering*. Englewood Cliffs, NJ: Prentice Hall.
Crouse, C.B., Hushmand, B., Luco, J.E. & Wong, H.L. 1990. Foundation impedance functions: theory versus experiment. *Journal of Geotechnical Engineering* 116(3): 432–449.
Crouse, C.B., Liang, G.C. & Martin, G.R. 1985. Experimental foundation impedance functions. *Journal of Geotechnical Engineering* 111(6): 819–822.
Crouse, C.B. & McGuire, J. 2001. Energy dissipation in soil-structure interaction. *Earthquake Spectra* 17 (2): 235–259.
Ghayoomi, M. & Wadsworth, S. 2014. Renovation and reoperation of a geotechnical centrifuge at the University of New Hampshire. *8th International Conference on Physical Modelling in Geotechnics*, 2014. Perth, Australia: CRC press.
Hushmand, B., Scott, R.F. & Crouse, C.B. 1988. Centrifuge liquefaction tests in a laminar box. *Géotechnique* 38(2): 253–262.
Kausel, E. 1974. *Forced vibrations of circular foundations on layered media*, Massachusetts Institute of Technology.
Kim, S. 2001. Calibration of simple models for seismic soil -structure interaction from field performance data, University of California, Los Angles.
Kim, S. & Stewart, J.P. 2003. Kinematic soil-structure interaction from strong motion recordings. *Journal of Geotechnical and Geoenvironmental Engineering* 129(4): 323–335.
Lin, A.N. & Jennings, P.C. 1984. Effect of embedment on foundation-soil impedances. *Journal of Engineering Mechanics* 110(7): 1060–1075.
Luco, J.E. & Wong, H.L. 1986. Response of a rigid foundation to a spatially random ground motion. *Earthquake Engineering & Structural Dynamics* 14(6): 891–908.
Mason, H.B., Kutter, B.L., Bray, J.D., Wilson, D.W. & Choy, B.Y. 2010. Earthquake motion selection and calibration for use in a geotechnical centrifuge. *7th International Conference on Physical Modeling in Geotechnics* Leiden, the Netherlands: CRC Press.
Menq, F. 2003. *Dynamic properties of sandy and gravelly soils*, The University of Texas at Austin.
Mirshekari, M., Ghayoomi, M. & Borghei, A. 2018. A review on soil-water retention scaling in centrifuge modeling of unsaturated sands. *Geotechnical Testing Journal* 41(6).
Moslem, K. & Trifunac, M.D. 1986. Effects of soil structure interaction on the response of building during the strong earthquake ground motion, *University of Southern California*: 1–158.
NEHRP CJV(Consultants Joint Venture), 2012. Soil-structure interaction for building structures, Washington, D.C.: *National Intuitive of Standards and Technology*: 1–292.
Poulos, H.G. & Davis, E.H. 1974. *Elastic solutions for soil and rock mechanics*. New York: John Wiley.
Rathje, E.M., Abrahamson, N.A. & Bray, J.D. 1998. Simplified frequency content estimates of earthquake ground motions. *Journal of Geotechnical and Geoenvironmental Engineering* 124(2): 150–159.
Seed, H.B. & Idriss, I.M. 1970. Soil moduli and damping factors for dynamic response analyses, Berkeley, California: *Earthquake engineering research center*.
Simulia 2012. Abaqus 6.12 Documentation, Rhode Island, USA: *Dassault Systemes Simulia Corp*.
Stewart, J.P., Fenves, G.L. & Seed, R.B. 1999. Seismic soil structure iteration in buildings. I: analytical methods. *Journal of Geotechnical and Geoenvironmental Engineering* 125: 26–37.
Stewart, J.P., Kim, S., Bielak, J., Dobry, R. & Power, M.S. 2003. Revisions to soil-structure interaction procedures in NEHRP design provisions. *Earthquake Spectra* 19(3): 677–696.
Veletsos, A.S., Prasad, A.M. & Wu, W.H. 1997. Transfer function for rigid rectangular foundation. *Earthquake Engineering & Structural Dynamics* 26(1): 5–17.
Veletsos, A.S. & Prasad, A.M. 1989. Seismic Interaction of Structures and Soils: Stochastic Approach. *Journal of Structural Engineering* 115(4): 935–956.
Veletsos, A.S. & Wei, Y.T. 1971. Lateral and rocking vibration of footings. *Journal of Soil Mechanics & Foundations Division* 97(9): 1227–1248.
Wolf, J. 1985. *Dynamic soil-structure interaction*. Englewood Cliffs, New Jersey: Prentice Hall, Inc.
Wong, H.L. & Luco, J.E. 1985. Tables of impedance functions for square foundations on layered media. *International Journal of Soil Dynamics and Earthquake Engineering* 4(2): 64–81.
Wong, H.L., Trifunac, M.D. & Luco, J.E. 1988. A comparison of soil-structure interaction calculations with results of full-scale forced vibration tests. *Soil Dynamics and Earthquake Engineering* 7(1): 22–31.
Wood, D.M. 2004. (1st) *Geotechnical modeling*. Florence: CRC Press.